Electron Spin Resonance and Electron Spin Echo Modulation Studies of Adsorbate Interactions with Cupric Ion on the Aluminum Content in Cu−AlMCM-41 Materials

Jie Xu,[†] Jong-Sung Yu,[‡] Seung Jae Lee,[‡] Bo Young Kim,[‡] and Larry Kevan*[,†]

Department of Chemistry, University of Houston, Houston, Texas 77204-5641, and Department of Chemistry, Hannam University, Taejon, Chungnam, 300-791, Korea

Received: October 21, 1999; In Final Form: December 7, 1999

Employing electron spin resonance (ESR) and electron spin echo modulation (ESEM) spectroscopy, adsorbate interactions are studied in two types of ion-exchanged Cu−AlMCM-41 materials. One is structurally ordered Cu−AlMCM-41(60)-I, Cu−AlMCM-41(40)-I, Cu−AlMCM-41(20)-I, and the other is less structurally ordered Cu−AlMCM-41(15)-II. Four Cu(II) species are observed by ESR. Species A with ESR parameters $g_{\|}^{A} = 2.406$, $A_{\|}^{A} = 0.0145$ cm^{-1}, and $g_{\perp}^{A} = 2.081$ is assigned to octahedral Cu(II) and is observed in hydrated Cu−AlMCM-41. Species B with $g_{\|}^{B} = 2.317$, $A_{\|}^{B} = 0.0176$ cm^{-1}, and $g_{\perp}^{B} = 2.076$ is assigned to distorted octahedral Cu(II) and is observed in dehydrated samples. Species C with $g_{\|}^{C} = 2.430$, $A_{\|}^{C} = 0.0125$ cm^{-1}, and $g_{\perp}^{C} = 2.091$ is also assigned to octahedral Cu(II) and is observed after adsorption of CH_3OD. Species D contains square planar D1 Cu(II) with $g_{\|}^{D1} = 2.280$, $A_{\|}^{D1} = 0.0168$ cm^{-1}, and $g_{\perp}^{D} = 2.058$, and distorted octahedral D2 Cu(II) with $g_{\|}^{D2} = 2.249$ and $A_{\|}^{D2} = 0.0190$ cm^{-1} after adsorption of ammonia. The accessibility to water, methanol, and ammonia adsorbates is similar for Cu(II) ions in Cu−AlMCM-41(60)-I, Cu−AlMCM-41(40)-I, and Cu−AlMCM-41(20)-I. This is confirmed by ESEM simulations which show that all Cu(II) in these samples coordinates to six D_2O or CH_3OD molecules. However, Cu(II) in Cu−AlMCM-41(15)-II is less accessible to adsorbates and interacts with two fewer D_2O or CH_3OD molecules than in Cu−AlMCM-41(*n*)-I samples. Therefore, the Cu(II) adsorption interactions do not depend on the Si/Al ratio but depend on structural ordering in different types of AlMCM-41 samples. This can be explained by different acidic sites in these types of AlMCM-41 materials.

Introduction

The investigation of ordered M41S type mesoporous silica molecular sieves is an active research area due to their variable pore diameters and topologies.[1−4] MCM-41 is the member of this novel family of materials with uniform hexagonal pores with diameters ranging from 20 Å to more than 100 Å.[1−13] These materials are possible new catalysts for large molecules.[1−4] Different transition metal ions have been ion-exchanged into silica MCM-41 and aluminosilica AlMCM-41 materials.[11−15] The incorporation of aluminum into the MCM-41 framework creates a negative framework charge and increases the ion exchange capacity.[13] As in zeolites and silicoaluminophosphate (SAPO-*n*) materials, such transition metal ions may offer specific sites for catalysis.[1−4,16]

To understand the catalytic potential of metal ions in MCM-41 materials detailed characterization of their environment and their interactions with adsorbates is required. Cu(II) exchanged silica MCM-41 (denoted Cu−MCM-41) and aluminosilica AlMCM-41 (Si/Al = 16) [denoted Cu−AlMCM-41(16)] materials were initially investigated.[11,12] It was found that cupric ions interact more strongly with AlMCM-41 than with MCM-41 because only four water molecules coordinate with Cu(II) in AlMCM-41 while Cu(II) in MCM-41 coordinates six water molecules. However, Kim et al.[14] later found that Cu−AlMCM-41 (Si/Al = 44) coordinates six water molecules. This difference in the adsorbate coordination number was attributed to superior structural organization in the Cu−AlMCM-41 prepared by Kim et al.[14] However, since these two AlMCM-41 materials had different Si/Al ratios and aluminum coordination, there is uncertainty if the Si/Al ratios and the aluminum coordination also affect the interactions between ion exchanged Cu(II) ions and adsorbates. Therefore, aluminosilica AlMCM-41 samples with only tetrahedral aluminum but with different Si/Al ratios and different degrees of structural organization were prepared in order to study their Cu(II) environment and the Cu(II) interactions with adsorbates.

Two types of liquid ion-exchanged Cu−AlMCM-41 materials were studied. One type has greater structural organization and is designated as Cu−AlMCM-41(*n*)-I, where I represents the synthesis method used and *n* stands for the Si/Al ratio. The other type of AlMCM-41 with poorer structural organization is designated as Cu−AlMCM-41(*n*)-II. The dehydration behavior and the interactions with adsorbates is studied by electron spin resonance (ESR) and electron spin echo modulation (ESEM).

Experimental Section

Synthesis. Two types of AlMCM-41 materials were synthesized. Type I with greater structural organization was synthesized by high-temperature synthesis method I.[14] Type II with poorer structural organization was synthesized by low-temperature synthesis method II.[15]

In synthesis method I, the structure-directing agent was an aqueous NH_3 surfactant solution containing dodecyltrimethylammonium bromide (DTAB), tetrapropylammonium bromide (TPAB), and cetyltrimethylammonium chloride (CTAC). The silica and alumina sources were colloidal silica and sodium aluminate. All these chemicals are from Aldrich Chemical.

[†] University of Houston.
[‡] Hannam University.

10.1021/jp993753k CCC: $19.00
Published on Web 01/26/2000

To make synthesis gels, the silicate solution and sodium aluminate solution were added dropwise into the surfactant solution with vigorous stirring at room temperature. The molar composition of the resulting gel mixture was 6.00 SiO_2/(0.06−0.20) Al_2O_3/1.00 CTAC/0.25 DTAB/0.25 TPAB/0.16 $(NH_4)_2O$/1.50 Na_2O/302 H_2O. After the gel mixture was hydrothermally crystallized at 373 K for 1 day, the reaction mixture was cooled to room temperature and the pH of the reaction mixture was adjusted to 10.2 by acetic acid. Then the reaction mixture was heated again to 373 K for 1 day. This procedure for pH adjustment and subsequent heating for 1 day was repeated twice more for a total of 4 days. The surfactant was first extracted by an ethanol−hydrochloric acid mixture (0.1 mol of HCl/L of ethanol) for 1 h under reflux conditions. Final calcination of the product was carried out in flowing O_2 at 813 K for 10 h. The resulting samples are denoted as AlMCM-41(*n*)-I where *n* is the Si/Al ratio in the gel and I (or II) refers to the synthesis method. The actual Si/Al ratios in the products AlMCM-41-(60)-I, AlMCM-41(40)-I, and AlMCM-41(20)-I are 66, 42, and 26, respectively. They were analyzed by a JEOL JXA-8600 electron microprobe.

In synthesis method II, 10 mL tetraethyl orthosilicate (Aldrich) was added to an aqueous solution containing 7 mL cationic surfactant CTAC (25% in H_2O from Aldrich Chemical) and 13.2 mL 2 M NaOH in 70 mL deionized water. $AlCl_3 \cdot 6H_2O$ (J. T. Baker Chemical) was added to this mixture as the aluminum source. The molar composition of the final gel mixture was SiO_2/(0−0.1) Al_2O_3/0.12 CTAC/0.15 Na_2O/139 H_2O. After stirring for 8 h at room temperature, crystallized AlMCM-41 was collected. The obtained as-synthesized samples were then calcined at 823 K in air for 24 h to remove the CTAC. The Si/Al ratio of AlMCM-41(15)-II was determined by electron microprobe analysis to be 11.

Liquid-state Cu(II) ion-exchanged samples were prepared by stirring 1 g of calcined AlMCM-41(*n*) in 100 mL of 0.002 M $Cu(CH_3COO)_2$ solution at room temperature for 6 h. The material was then filtered and washed at 343 K by deionized water in order to remove any ions adsorbed on the external surface. These ion-exchanged samples are designated as Cu−AlMCM-41(*n*)-I (or II) where *n* is the Si/Al ratio in the gel.

Characterization. Powder X-ray powder diffraction (XRD) patterns were collected using a Philips 1840 powder diffractometer with Cu Kα radiation (40 kV, 25 mA) at 0.025° step size and 1 s step time over a $1.5° < 2\theta < 10°$ range. The samples were prepared as thin layers on metal slides.

N_2 adsorption isotherms were measured at 77 K using a Micromeritics Gemini 2375 analyzer. The volume of adsorbed N_2 was normalized to standard temperature and pressure. Prior to adsorption, the samples were dehydrated at 573 K for 5 h. The specific surface area, A_{BET}, was determined from the linear part of the BET equation. The pore size distribution was calculated from the desorption branches of the N_2 adsorption isotherm using the Barrett−Joyner−Halenda (BJH) formula.[17−19]

For ESR and ESEM measurements, fresh, hydrated samples were loaded into 3 mm o.d. by 2 mm i.d. Suprasil quartz tubes. Completely dehydrated samples are obtained by the following procedure. The sample was evacuated ($P < 10^{-4}$ Torr) at 293 K for 14 h, then subsequently heated at 393 K for 14 h and at 623 K for 4 h in a vacuum and finally heated under oxygen (50−100 Torr) at 623 K for 10 h. Adsorption was done by exposing dehydrated samples to D_2O (Aldrich) and CH_3OD (Stohler Isotope Chemicals) at their room-temperature vapor pressures for 14 h. ND_3 and $^{15}NH_3$ (Cambridge Isotope Laboratories) were adsorbed at 40 Torr for 6 h.

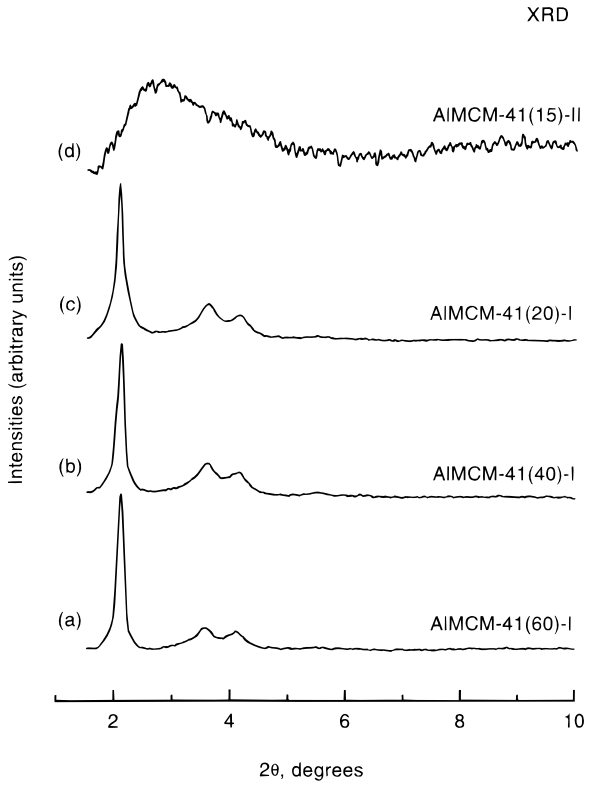

Figure 1. Powder XRD patterns of calcined AlMCM-41 materials (a) Cu−AlMCM-41(60)-I, (b) Cu−AlMCM-41(40)-I, (c) Cu−AlMCM-41(20)-I, and (d) Cu−AlMCM-41(15)-II. (a−c) are obtained by method I and (d) is synthesized by method II.

X-band (9 GHz) ESR spectra were recorded at 77 K on a Bruker ESP 300 spectrometer. The relative ESR intensities were calculated by double integration of the recorded ESR signals. The ESEM modulations were recorded at 4 K on an ESP 380 Bruker FT ESR spectrometer using a $\pi/2-\tau-\pi/2-T-\pi/2$ pulse sequence as a function of T.[20] Different values of τ in a three-pulse experiment were selected to minimize the ^{27}Al modulation.[20] The time-domain deuterium ESEM modulation was analyzed by a spherical approximation for powder samples in terms of N nuclei at distance R with an isotropic hyperfine coupling A_{iso} where the modulation function was simulated and fitted to the experimental data by a least squares procedure.[21]

Results

XRD and ^{27}Al MAS NMR. An XRD pattern characteristic of the MCM-41 structure[3,4] is observed for calcined Cu−AlMCM-41(60)-I, Cu−AlMCM-41(40)-I, and Cu−AlMCM-41-(20)-I as shown in Figure 1a−c. All three samples prepared by synthesis method I show a strong narrow d_{100} peak and the 110 and 200 reflections are well resolved. These support that a highly ordered hexagonal mesostructure is obtained.[8,10] In contrast, calcined Cu−AlMCM-41(15)-II which is synthesized by method II only shows a broad d_{100} peak near 2.5° 2θ and the 110 and 200 reflections are not resolved (Figure 1d). This indicates that Cu−AlMCM-41(15)-II is less structurally ordered than Cu−AlMCM-41-I. However, all samples show only a single peak around 54 ppm relative to $Al(H_2O)_6^{3+}$ in their ^{27}Al MAS NMR spectra (not shown).[14,15] This peak position indicates that all aluminum is tetrahedrally coordinated in these two types of AlMCM-41 materials.[22,23]

N_2 Adsorption Isotherms. Low-temperature nitrogen adsorption isotherms enable the calculation of the specific surface

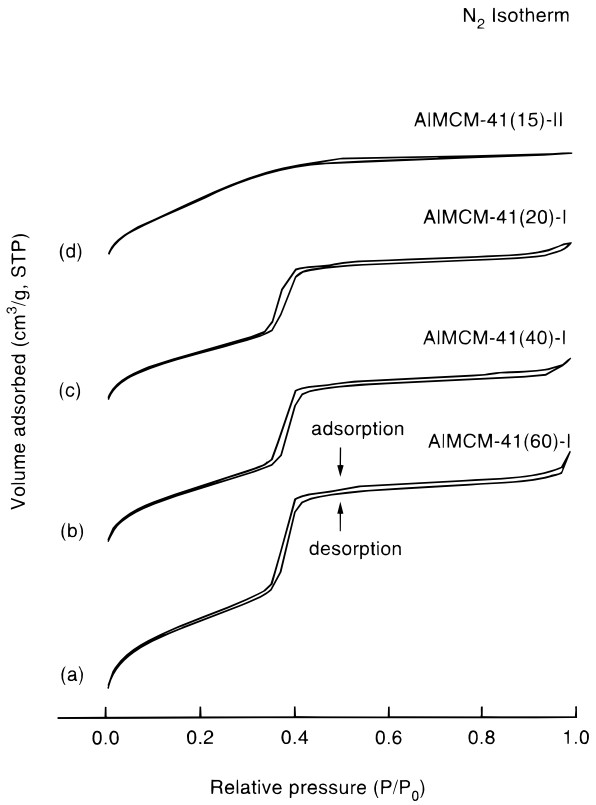

Figure 2. Nitrogen adsorption−desorption isotherms at 77 K: (a) Cu−AlMCM-41(60)-I; (b) Cu−AlMCM-41(40)-I; (c) Cu−AlMCM-41(20)-I; (d) Cu−AlMCM-41(15)-II.

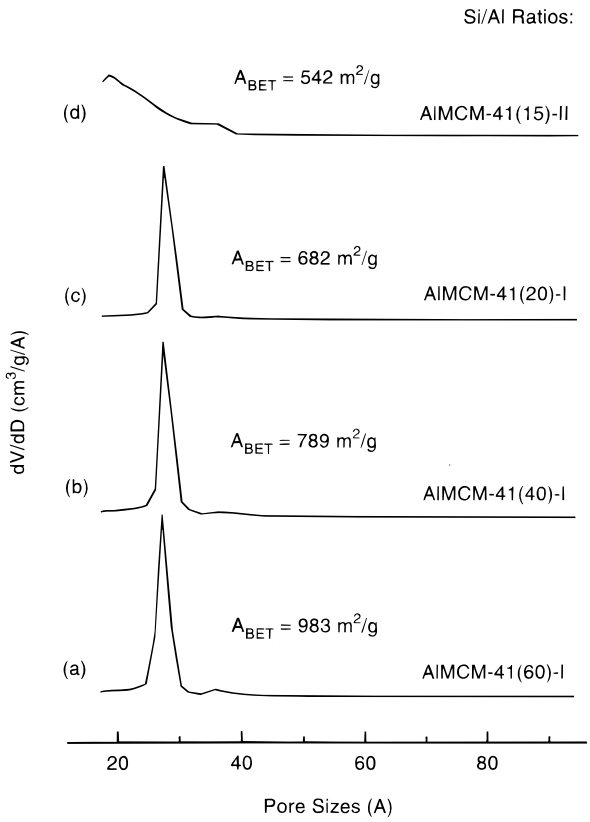

Figure 3. Pore size distributions calculated by the Barrett−Joyner−Halenda (BJH) formula: (a) Cu−AlMCM-41(60)-I; (b) Cu−AlMCM-41(40)-I; (c) Cu−AlMCM-41(20)-I; (d) Cu−AlMCM-41(15)-II.

area and mesopore size distribution. The N_2 adsorption isotherms for the calcined Cu−AlMCM-41(60)-I, Cu−AlMCM-41(40)-I, and Cu−AlMCM-41(20)-I materials are shown in Figure 2a−c. They are typical reversible type IV adsorption isotherms as defined by IUPAC.[24] The sharp inflection between relative pressure $P/P_0 = 0.2$ and 0.3 corresponds to capillary condensation within uniform mesopores. The sharpness of this step reflects the uniform pore size. Therefore, a very uniform mesopore system is observed in calcined Cu−I-*n* materials, which is consistent with their XRD patterns. In contrast, no obvious inflection is observed in the N_2 adsorption isotherms for the calcined Cu−AlMCM-41(15)-II as shown in Figure 2d. This indicates that Cu−AlMCM-41(15)-II is less structurally ordered, which is also consistent with its XRD pattern.

The BJH plots of the derivative of the pore volume per unit weight with respect to the pore diameter (d*V*/d*D*) versus the pore diameter are shown in Figure 3. A very narrow pore size distribution with a pore diameter of around 24 Å is observed in Cu−AlMCM-41(60)-I, Cu−AlMCM-41(40)-I, and Cu−AlMCM-41(20)-I samples (Figure 3a−c). Their surface areas are near or over 700 m^2/g. Therefore, all Cu−I-*n* samples possess a very uniform pore structure and high surface area. However, Cu−AlMCM-41(15)-II has a very broad pore size distribution extending from about 42 Å to lower values (Figure 3d). Therefore, this sample has less uniform pores even though its surface area is as high as 542 m^2/g.

ESR. The Cu(II) ion-exchanged Cu−AlMCM-41 samples were studied by ESR at the stages of fresh hydrated, dehydrated, and oxygen oxidized and with subsequently adsorbed water, methanol, and ammonia. To obtain well-resolved ESR spectra, the copper concentrations are controlled to a Si/Cu ratio of around 1000 in these samples.

The ESR spectra of fresh, hydrated Cu(II) ion-exchanged samples are shown in Figure 4. At 293 K, Cu−AlMCM-41-(60)-I and Cu−AlMCM-41(20)-I show one isotropic line centered at $g_{iso} = 2.190$ with peak-to-peak line width of about 139 G (parts a and b of Figure 4), indicating the existence of a mobile Cu(II) species. Cu−AlMCM-41(40)-I also shows a similar spectrum (not shown). In contrast, fresh, hydrated Cu−AlMCM-41(15)-II gives a spectrum with two superposed species at 293 K (Figure 4c). One is a broad isotropic peak near $g_{iso} = 2.190$, corresponding to a mobile Cu(II) species. The other appears axially symmetric near $g_\perp = 2.081$. However, at 77 K, all these samples give a spectrum like Cu−AlMCM-41(20)-I shown in Figure 4d. Only one axially symmetric species A with ESR parameters $g_{||}^A = 2.406$, $A_{||}^A = 0.0145\ cm^{-1}$, and $g_\perp^A = 2.081$ is observed. Four peaks in the $g_{||}$ region are due to the hyperfine splitting of copper nuclei ($I = {}^3/_2$). No splitting in the $g_\perp$ region is resolved.

The ESR spectra obtained after dehydration and oxidization at 623 K are shown in Figure 5. The signal of species A disappears and a new species B is produced. At 293 K, Cu−AlMCM-41(60)-I, Cu−AlMCM-41(20)-I, and Cu−AlMCM-41-(15)-II show similar anisotropic ESR signals with hyperfine splittings on $g_\perp$ (Figure 5a−c). Cu−AlMCM-41(40)-I also shows a similar spectrum (not shown). Like Cu−AlMCM-41-(20)-I shown in Figure 5d, at 77 K all samples give an axially symmetric signal B with ESR parameters $g_{||}^B = 2.317$, $A_{||}^B = 0.0176\ cm^{-1}$, and $g_\perp^B = 2.076$. The Cu(II) hyperfine splittings in the $g_\perp$ region can be resolved now, and only one ESR species is identified at both 293 and 77 K.[12,25]

Rehydration of these dehydrated samples by D_2O recovers the fresh, hydrated ESR spectra (not shown) like those in Figure 4. At 293 K, rehydrated Cu−AlMCM-41(60)-I, Cu−AlMCM-41(40)-I, and Cu−AlMCM-41(20)-I only show a broad symmetric ESR peak at $g_{iso} = 2.190$, which is similar to the spectra in parts a and b of Figure 4. However, rehydrated Cu−AlMCM-

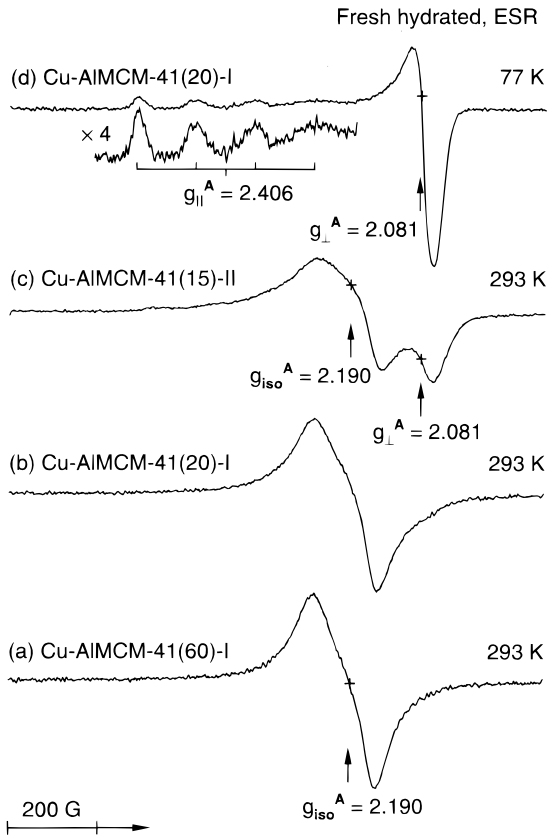

Figure 4. ESR spectra of fresh, hydrated Cu−AlMCM-41: (a) Cu−AlMCM-41(60)-I at 293 K; (b) Cu−AlMCM-41(20)-I at 293 K; (c) Cu−AlMCM-41(15)-II at 293 K; (d) Cu−AlMCM-41(20)-I at 77 K.

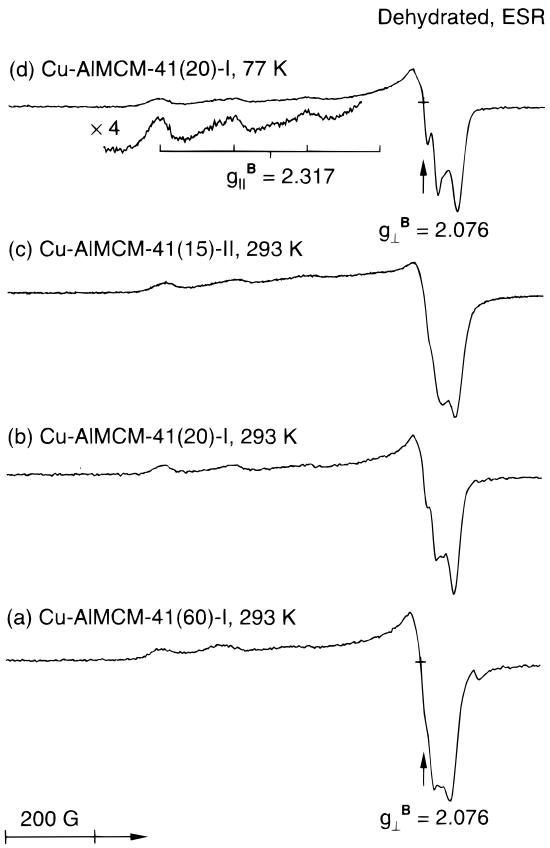

Figure 5. ESR spectra of dehydrated Cu−AlMCM-41: (a) Cu−AlMCM-41(60)-I at 293 K; (b) Cu−AlMCM-41(20)-I at 293 K; (c) Cu−AlMCM-41(15)-II at 293 K; (d) Cu−AlMCM-41(20)-I at 77 K.

41(15)-II shows a signal comprised of an isotropic peak near $g_{iso} = 2.190$ and an axially symmetric peak around $g_{\perp} = 2.081$ at 293 K, which is same as for fresh, hydrated Cu−AlMCM-41(15)-II in Figure 4c. Also, all samples only show an anisotropic species A at 77 K.

After dehydrated samples are exposed to CH_3OD at room temperature for 14 h, a new species C with the ESR parameters $g_{\|}^{C} = 2.430$, $A_{\|}^{C} = 0.0125$ cm^{-1}, and $g_{\perp}^{C} = 2.091$ is observed as shown in Figure 6. At 293 K, Cu−AlMCM-41(60)-I and Cu−AlMCM-41(20)-I show ESR signals comprised of an isotropic peak at $g_{iso} = 2.195$ and an axially symmetric peak around $g_{\perp} = 2.091$ (parts a and b of Figure 6). So some Cu(II) ions are less mobile than others. A similar spectrum is also observed in Cu−AlMCM-41(40)-I (not shown). Unlike Cu−AlMCM-41-I samples, Cu−AlMCM-41(15)-II with adsorbed CH_3OD only shows an anisotropic ESR signal at 293 K (Figure 6c), suggesting only the existence of less mobile Cu(II) ions. However, at 77 K, Cu−AlMCM-41(20)-I with adsorbed CH_3OD shows axially symmetric species C as shown in Figure 6d. Exactly the same ESR spectrum is observed at 77 K in Cu−AlMCM-41(60)-I, Cu−AlMCM-41(40)-I, and Cu−AlMCM-41(15)-II with adsorbed CH_3OD. So there is only one Cu(II) species in these samples.

The adsorption of ammonia on dehydrated Cu−AlMCM-41(20)-I at room temperature results in a new ESR species D as shown in Figure 7. The color of the sample is light blue. Figure 7a is the spectrum obtained at 293 K after adsorbing $^{15}NH_3$. Only an anisotropic signal is observed. Its 77 K ESR spectrum is shown in Figure 7b. Two overlapping Cu(II) species D1 and D2 in the $g_{\|}$ region are observed. The ESR parameters are $g_{\|}^{D1} = 2.280$ and $A_{\|}^{D1} = 0.0168$ cm^{-1} for species D1 and $g_{\|}^{D2} = 2.249$ and $A_{\|}^{D2} = 0.0190$ cm^{-1} for species D2. Species D2 decreases in intensity with time. A similar result was observed by Kim et al.[14] The hyperfine splittings in the $g_{\perp}$ region are due to ^{15}N nuclei ($I = {}^1/_2$). So only an average $g_{\perp}^{D} = 2.058$ can be determined. The second derivative spectrum of the $g_{\perp}$ region is shown in Figure 7c, where five ^{15}N hyperfine lines with peak-to-peak line width 0.0007 cm^{-1} and hyperfine coupling $A^{N} = 0.0018$ cm^{-1} centered at $g = 2.045$ are observed. These couplings are consistent with $A^{N} = 0.0019$ cm^{-1} found in siliceous Cu−MCM-41.[11] The intensity ratio of the five ^{15}N hyperfine peaks is close to 1:4:6:4:1, which indicates that four equivalent $^{15}NH_3$ molecules interact with Cu(II) in Cu−AlMCM-41(20)-I. To verify this result, Cu−AlMCM-41(20)-I with adsorbed $^{14}NH_3$ ($I = 1$) was also recorded by ESR at 77 K. The resulting second derivative ESR spectrum is shown in Figure 7d. Nine ^{14}N hyperfine peaks with the expected intensity ratio are observed in the $g_{\perp}$ region. This supports that Cu(II) ions in Cu−AlMCM-41(20)-I coordinate with four ammonia molecules. Cu−AlMCM-41(60)-I and Cu−AlMCM-41(40)-I also show similar ESR spectra.

The ESR spectrum of Cu−AlMCM-41(15)-II with adsorbed $^{15}NH_3$ is shown in Figure 8. An anisotropic ESR signal is also observed at 293 K (Figure 8a). At 77 K, the D2 species and a trace of the D1 species marked by stars (*) together with ^{15}N hyperfine splittings are observed (Figure 8b). The second derivative spectrum is shown in Figure 8c and also gives five ^{15}N hyperfine lines with peak-to-peak line width 0.0007 cm^{-1} and $A^{N} = 0.0018$ cm^{-1} in the $g_{\perp}$ region, indicating that Cu(II) ions in Cu−AlMCM-41(15)-II are also coordinated to four ammonia molecules. However, compared to the spectrum of Cu−AlMCM-41(20)-I in Figure 7c, the relative intensity of the ^{15}N hyperfine splittings to the whole spectrum is much lower in Cu−AlMCM-41(15)-II since both have the same line width.

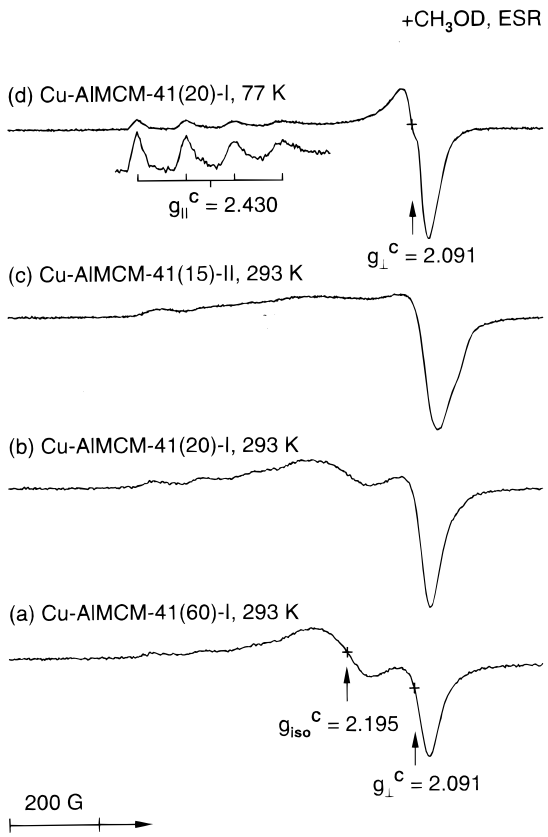

Figure 6. ESR spectra of Cu−AlMCM-41 with adsorbed methanol: (a) Cu−AlMCM-41(60)-I at 293 K; (b) Cu−AlMCM-41(20)-I at 293 K; (c) Cu−AlMCM-41(15)-II at 293 K; (d) Cu−AlMCM-41(20)-I at 77 K.

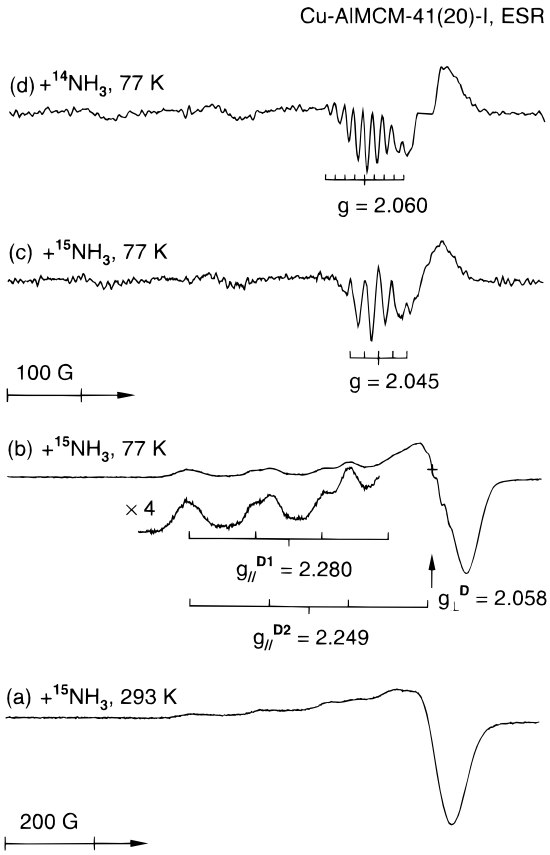

Figure 7. ESR spectra of Cu−AlMCM-41(20)-I with adsorbed ammonia: (a) $^{15}NH_3$ at 293 K; (b) $^{15}NH_3$ at 77 K; (c) second derivative spectrum of (b); (d) second derivative spectrum with $^{14}NH_3$ at 77 K.

ESEM. ESEM measurements of deuterium modulation of the Cu(II) ions were performed to identify the numbers of interacting molecules in the two types of Cu(II) ion exchanged AlMCM-41 materials. All ESEM spectra were recorded at the $g_\perp$ spectral region of the Cu(II) powder spectrum. The three-pulse ESEM spectrum of Cu−AlMCM-41(60)-I with adsorbed D_2O is shown in Figure 9a. A two-shell model is necessary to simulate the deuterium modulation in this system. The simulation shows one set of eight deuteriums interacting at a distance of 0.28 nm and a second set of four deuteriums interacting at a distance of 0.33 nm. This indicates that six water molecules are directly coordinated to Cu(II) in Cu−AlMCM-41(60)-I. The same result is obtained for adsorbed CH_3OD (Figure 9b). Four nearest-neighbor CH_3OD molecules are directly coordinated to Cu(II) at a Cu(II)−D distance of 0.28 nm and two more CH_3OD molecules interact at a Cu(II)−D distance of 0.34 nm.

The three-pulse ESEM spectra of Cu−AlMCM-41(40)-I and Cu−AlMCM-41(20)-I with adsorbed D_2O and CH_3OD are similar to those of Cu−AlMCM-41(60)-1. Thus, the Si/Al ratio does not affect the adsorbate coordination.

The three-pulse ESEM spectra of Cu−AlMCM-41(15)-II with adsorbed D_2O and CH_3OD are shown in Figure 10. For adsorbed D_2O in Figure 10a, the simulation shows six deuteriums at 0.28 nm and two deuteriums at 0.32 nm interacting with Cu(II). This indicates that three waters directly coordinate to Cu(II) and one water interacts at a longer distance. Different results are obtained from simulations of three-pulse ESEM spectra with adsorbed CH_3OD (Figure 10b). Two CH_3OD directly coordinate to Cu(II) and two more CH_3OD interact at a longer distance.

The ESEM simulation parameters for Cu-containing AlMCM-41 are summarized in Table 1. Six water or methanol molecules interact with Cu(II) in Cu−AlMCM-41(60)-I, Cu−AlMCM-41(40)-I, and Cu−AlMCM-41(20)-I materials. However, only four water or methanol molecules interact with Cu(II) in Cu−AlMCM-41(15)-II.

Discussion

The two types of AlMCM-41 samples are different in structural uniformity. Cu−AlMCM-41-I samples possess well-defined hexagonal mesostructures confirmed by their XRD patterns (Figure 1a−c) and narrow pore size distributions (Figure 3a−c). In contrast, Cu−AlMCM-41(15)-II has a less ordered mesostructure indicated by a poorer XRD pattern (Figure 1d) and a broader pore size distribution (Figure 3d), although its surface area is reasonably high. In addition, ^{27}Al MAS NMR spectra indicate that all aluminum in these two types of AlMCM-41 samples has tetrahedral coordination consistent with framework sites.

Cu(II) ESR parameters are different for Cu−AlMCM-41 after dehydration, oxidization, and subsequent adsorption of water, methanol, and ammonia. In general, $A_{||}$ increases from ∼0.007 cm^{-1} for tetrahedral symmetry, through distorted octahedral and square pyramidal symmetry, to ∼0.017 cm^{-1} for square-planar symmetry, whereas $g_{||}$ decreases from 2.516 to 2.245 for this sequence of coordination symmetries.[26,27] Therefore, based on the ESR parameters and ESEM simulation results, the possible coordination and location of Cu(II) ions may be deduced.

Cu(II) ESR Species. Four Cu(II) species have been observed in Cu(II) ion-exchanged AlMCM-41 materials. Species A is observed in fresh hydrated or rehydrated Cu−AlMCM-41-I. At 293 K, this species shows an isotropic ESR signal (parts a and c of Figure 4). This indicates that this Cu(II) species is a mobile

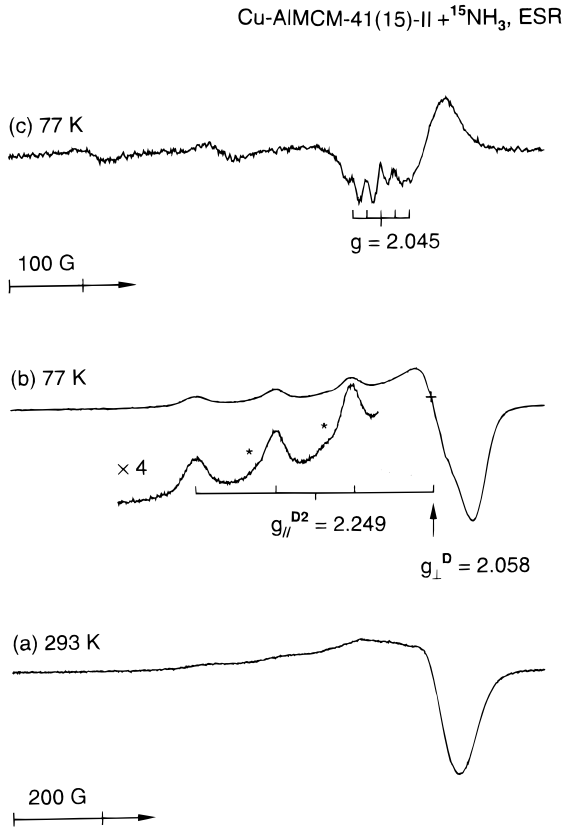

Figure 8. ESR spectra of Cu−AlMCM-41(15)-II with adsorbed $^{15}NH_3$ (a) at 293 K, (b) at 77 K, and (c) second derivative spectrum of (b).

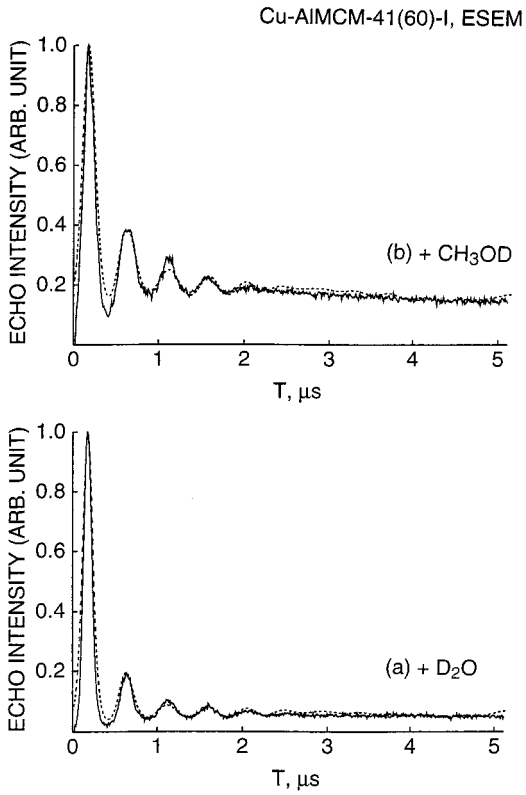

Figure 9. Experimental (—) and simulated (- - -) three-pulse ESEM at 4 K of Cu−AlMCM-41(60)-I with adsorbed (a) D_2O and (b) CH_3OD (t = 256 ns).

species which freely rotates on the ESR time scale. A similar broad isotropic ESR signal has been observed at room temperature for Cu(II) in zeolites and was assigned to $[Cu(H_2O)_6]^{2+}$ from ESR and ESEM analyses.[28−30] Therefore, species A is assigned to octahedrally symmetric Cu(II) ions located in a main channel of AlMCM-41. At 77 K, species A becomes less mobile and shows an anisotropic spectrum (Figure 4d).

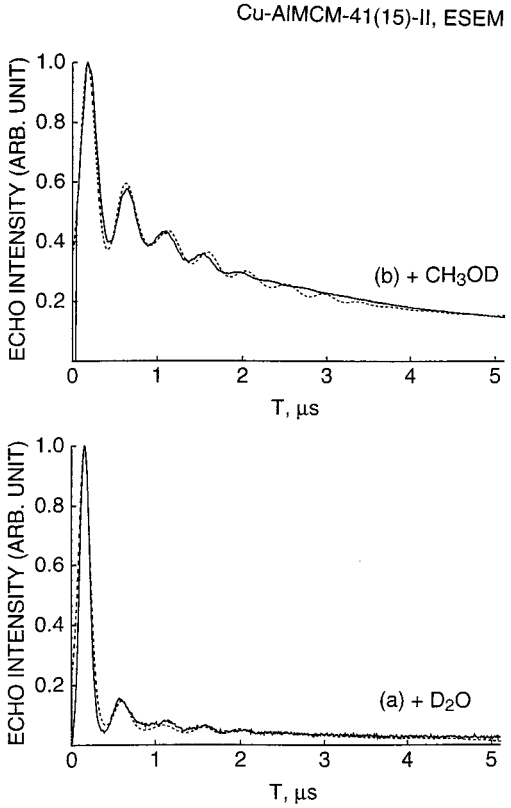

Figure 10. Experimental (—) and simulated (- - -) three-pulse ESEM at 4 K of Cu−AlMCM-41(15)-II with adsorbed (a) D_2O and (b) CH_3OD (t = 256 ns).

TABLE 1: Simulation Parameters for Three-Pulse ESEM of Cu(II) in Cu−AlMCM-41 Materials with Adsorbates

samples	adsorbate	shell	N^a	R (nm)^b	A_{iso} (MHz)^c	number of adsorbates
Cu−AlMCM-41(60)-I	D_2O	1	8	0.28	0.21	4
		2	4	0.33	0.13	2
	CH_3OD	1	4	0.28	0.20	4
		2	2	0.34	0.12	2
Cu−AlMCM-41(40)-I	D_2O	1	8	0.28	0.20	4
		2	4	0.32	0.09	2
	CH_3OD	1	4	0.28	0.15	4
		2	2	0.34	0.08	2
Cu−AlMCM-41(20)-I	D_2O	1	8	0.28	0.23	4
		2	4	0.34	0.11	2
	CH_3OD	1	4	0.28	0.10	4
		2	2	0.32	0.10	2
Cu−AlMCM-41(15)-II	D_2O	1	6	0.28	0.25	3
		2	2	0.32	0.06	1
	CH_3OD	1	2	0.28	0.35	2
		2	2	0.31	0.14	2

[a] Number of ^2D nuclei. [b] Cu(II)-^2D distance. [c] Isotropic hyperfine coupling of ^2D nuclei.

Species B is obtained from dehydrated samples. It shows anisotropic ESR spectra at both 293 and 77 K. This indicates that these Cu(II) ions become immobile by losing coordinated water and are likely coordinated to lattice oxygens. Compared to species A, species B has a smaller $g_{||}$ and a bigger $A_{||}$, consistent with a distorted octahedral symmetry.[14] Therefore, Cu(II) species B in dehydrated samples is likely located on the internal surface of a mesopore coordinated to lattice oxygens.

Species C is observed after adsorption of methanol onto dehydrated samples (Figure 6). It is also assigned to octahedral symmetry since it has an isotropic line at 293 K and only one species is observed at 77 K.

Species D is obtained from dehydrated samples upon adsorbing ammonia. There are two overlapping species in the $g_{||}$ region. One species with $g_{||}^{D1} = 2.280$ and $A_{||}^{D1} = 0.0168$ cm^{-1} (Figure 8) is tentatively assigned to a square planar tetraammonia complex $[Cu(NH_3)_4]^{2+}$ based on the ESR parameters obtained in similar systems.[11,14,31−33] The other species with $g_{||}^{D2} = 2.249$ and $A_{||}^{D2} = 0.0190$ cm^{-1} is possibly an intermediate structure between distorted octahedral and square planar geometry.[14] It is noted that the relative intensity of the D1 species to the overall spectrum in Cu−AlMCM-41(15)-II is weaker than in Cu−AlMCM-41(20)-I.

Adsorbate Coordination Dependence on Si/Al. The interactions between Cu(II) ions in Cu−AlMCM-41(*n*)-I and adsorbates are studied by ESR and ESEM techniques. Hydrated or rehydrated Cu−AlMCM-41(60)-I, Cu−AlMCM-41(40)-I, and Cu−AlMCM-41(20)-I all show an isotropic symmetric ESR signal at 293 K (Figure 4a−c) and an axially symmetric species A at 77 K. So Cu(II) ions show some accessibility to water in these samples. The ESEM measurements of deuterium modulation also indicate that six water molecules are coordinated to the Cu(II) ions in these materials (Table 1). This suggests weak bonding of Cu(II) ions to the ion exchange sites in Cu−AlMCM-41(*n*)-I. And, the adsorbate interaction of D_2O is not dependent on the Si/Al ratio.

The adsorbate interaction of methanol on dehydrated Cu−AlMCM-41(*n*)-I samples is also independent of the Si/Al ratio. All Cu−AlMCM-41(*n*)-I samples with adsorbed CH_3OD show an isotropic peak overlapped by another anisotropic peak at 293 K (parts a and b of Figure 6) but only one species C is obtained at 77 K. So all Cu(II) ions in these samples show a similar accessibility to CH_3OD. ESEM simulations also indicate that six methanol molecules are coordinated to Cu(II) ions in these samples (Table 1). The adsorption of methanol is also not affected by the Si/Al ratio.

The adsorption of ammonia on Cu−AlMCM-41(*n*)-I also shows the same behavior. All samples show similar anisotropic ESR spectra at 193 K (Figure 7a), indicating similar accessibility to ammonia. The second derivative ESR spectra with adsorbed $^{15}NH_3$ and $^{14}NH_3$ show that Cu(II) ions interact with four ammonia molecules to form $[Cu(NH_3)_4]^{2+}$ (parts c and d of Figure 7). The nitrogen splitting observed in Figure 7 indicates that Cu(II) ions in these samples strongly coordinate to ammonia. Therefore, the adsorption of ammonia on these samples is also not influenced by the Si/Al ratio.

The fact that the adsorbate interactions with Cu(II) in Cu−AlMCM-41(*n*)-I are independent of the framework aluminum content is reasonable. The interactions between Cu(II) and adsorbates should be mainly determined by the interactions between Cu(II) and the oxygens in the AlMCM-41 framework. In AlMCM-41 materials, the incorporation of aluminum into the framework generates Brönsted acid sites which may act as ion exchange sites. The interaction between cationic Cu(II) and such ion exchange sites is determined by the negative charge on the oxygens near a Brönsted acid site which is regulated by a nearby aluminum.[34−36] Each tetrahedrally coordinated framework aluminum contributes −0.25 net charge at surface hydroxyl groups and −1.25 net charge at surface oxygens in aluminas.[37] Each aluminum in Cu−AlMCM-41(*n*)-I will contribute the same amount of negative charge to the nearby oxygens at an ion exchange site. Since the aluminums are isolated, the interaction of Cu(II) to framework oxygens should be independent of the Si/Al ratio. Also, in zeolites the Brönsted acidity becomes constant with an increase of aluminum content for Si/Al ratios more than 6.[36,38] So no adsorption dependence on the Si/Al ratio is expected in Cu−AlMCM-41 materials.

This conclusion is also supported by the data on type II samples with a different Si/Al ratio. As indicated by the ESR and ESEM results, Cu(II) ions in Cu−AlMCM-41(15)-II interact only with four D_2O, CH_3OD, and NH_3 molecules. Our former studies on Mn-containing AlMCM-41-(62) materials synthesized at room temperature (type II synthesis) indicate that Mn(II) ions in Mn−AlMCM-41-(62) also interact with four adsorbate molecules.[15]

Adsorbate Dependence on Structural Ordering. ESR and ESEM data indicate that the interactions of Cu(II) in Cu−AlMCM-41(15)-II with adsorbates are different from those in Cu−AlMCM-41(*n*)-I. Rehydrated Cu−AlMCM-41(15)-II shows a superposition of one isotropic peak and one anisotropic peak at 293 K (Figure 4c) while rehydrated Cu−AlMCM-41(20)-I only shows an isotropic signal (Figure 4a). Also, Cu−AlMCM-41(15)-II with adsorbed CH_3OD shows an anisotropic ESR signal at 293 K (Figure 6c), while Cu−AlMCM-41(20)-I shows an isotropic signal (Figure 6a). So the Cu(II) ions Cu−AlMCM-41(15)-II are less accessible to D_2O and CH_3OD than those in Cu−AlMCM-41(20)-I. ESEM simulation also indicates that two fewer water or methanol molecules are coordinated to Cu(II) ions in Cu−AlMCM-41(15)-II than in Cu−AlMCM-41(n)-I. Therefore, unlike Cu−AlMCM-41(*n*)-I samples, Cu(II) ions in Cu−AlMCM-41(15)-II are likely coordinated to two framework oxygens in addition to water or methanol.

The adsorption of ammonia on Cu−AlMCM-41(15)-II and Cu−AlMCM-41(*n*)-I is also different. Although Cu(II) ions in both material types with adsorbed $^{15}NH_3$ are immobile, the relative intensity of the Cu(II) D1 species to the overall spectrum in Cu−AlMCM-41(15)-II is lower than that in Cu−AlMCM-41(20)-I. Because the intensity of the nitrogen splittings is determined by the Cu−N coupling, the weaker intensity of ^{15}N hyperfine lines in Cu−AlMCM-41(15)-II suggests that Cu(II) ions in Cu−AlMCM-41(15)-II interact with ammonia more weakly than those in Cu−AlMCM-41(*n*)-I. Therefore, the Cu(II) ions in Cu−AlMCM-41(15)-II seem less accessible to ammonia than those in Cu−AlMCM-41(20)-I.

The adsorbate difference between Cu−AlMCM-41(*n*)-I and Cu−AlMCM-41(15)-II is likely due to the difference in structural order. Since the Si/Al ratios in Cu−AlMCM-41(20)-I and Cu−AlMCM-41(15)-II are comparable and all the aluminum is tetrahedral, the only difference between these two samples is structural ordering. The less ordered framework of Cu−AlMCM-41(15)-II may have more defects with increased silanol acidity,[39,40] which provide ion exchange sites. Compared to Brönsted acid sites, these sites should be located more on internal surfaces of the mesoporous structure and be less accessible to adsorbates. This is consistent with the observation by Kim et al.[14]

Conclusions

From ESR and ESEM studies on different Cu(II) ion-exchanged AlMCM-41 materials, four Cu(II) species are found and assigned to different symmetries. Species A is assigned to octahedral symmetry observed in hydrated samples. Species B is assigned to distorted octahedral or square pyramidal symmetry obtained in dehydrated samples. Species C is distorted octahedral Cu(II) produced upon adsorption of methanol. Species D is probably square-planar Cu(II) or has distorted octahedral symmetry upon adsorbing ammonia.

The interactions between ion exchanged Cu(II) ions and adsorbates are not dependent on the Si/Al ratio in the AlMCM-41 materials with good structural ordering but they are dependent on the structural ordering. The ion exchanged Cu(II) ions in well structured AlMCM-41 samples interact with adsorbates more strongly and show higher coordination numbers than in less well structured AlMCM-41.

Acknowledgment. This research was supported by the Robert A. Welch Foundation, the University of Houston Energy Laboratory, and the National Science Foundation. J.S.Y. thanks the Korea Science and Engineering Foundation (97-05-02-06-01-3) and the Korean Ministry of Science and Technology (1997) for support.

References and Notes

(1) Casci, J. L. In *Advanced Zeolite Science and Application*; Jansen, J. C., Stöcker, M., Karge, H. G., Weitkamp, J., Eds.; Elsevier: Amsterdam, 1994; p 329 [*Stud. Surf. Sci. Catal.* **1994**, *85*, 329].
(2) Sayari, A. *Chem. Mater.* **1996**, *8*, 1840.
(3) Corma, A. *Chem. Rev.* **1997**, *97*, 2373.
(4) Notari, B. *Catal. Today* **1993**, *18*, 163.
(5) Kresge, C. T.; Leonowicz, M. E.; Roth, W. J.; Vartuli, J. C.; Beck, J. S. *Nature* **1992**, *359*, 710.
(6) Beck, J. S.; Vartuli, J. C.; Roth, W. J.; Leonowicz, M. E.; Kresge, C. T.; Schmitt, K. D.; Chu, C. T.-W.; Olson, D. H.; Sheppard, E. W.; McCullen, S. B.; Higgins, J. B.; Schlenker, J. L. *J. Am. Chem. Soc.* **1992**, *114*, 10834.
(7) Huo, Q.; Margolese, D. I.; Ciesla, U.; Feng, P.; Gier, T. E.; Sieger, P.; Leon, R. Petroff, P. M.; Schüth, F.; Stucky, G. D. *Nature* **1994**, *368*, 317.
(8) Bagshaw, S. A.; Prouzet, E.; Pinnavaia, T. J. *Science* **1995**, *269*, 1242.
(9) Huo, Q.; Margolese, D. I.; Stucky, G. D. *Chem. Mater.* **1996**, *8*, 1147.
(10) Chen, C. Y.; Li, H. X.; Davis, M. *Microporous Mater.* **1993**, *2*, 17.
(11) Pöppl, A.; Newhouse, M.; Kevan, L. *J. Phys. Chem.* **1995**, *99*, 10019.
(12) Pöppl, A.; Hartmann, M.; Kevan, L. *J. Phys. Chem.* **1995**, *99*, 17251.
(13) Luan, Z.; Xu, J.; Kevan, L. *Nukleonika* **1997**, *42*, 493.
(14) Kim, J. Y.; Yu, J. S.; Kevan, L. *Mol. Phys.* **1998**, *95*, 989.
(15) Xu, J.; Luan, Z.; Wasowicz, T.; Kevan, L. *Microporous Mesoporous Mater.* **1998**, *22*, 179.
(16) Maxwell, J. E. *Adv. Catal.* **1982**, *31*, 1.
(17) Barrrett, E. P.; Joyner, L. G.; Halenda, P. P. *J. Am. Chem. Soc.* **1951**, *73*, 373.
(18) Tanev, P. T.; Vlaev, L. T. *J. Colloid Interface Sci.* **1993**, *160*, 110.
(19) Naono, H.; Hakuman, M.; Nakal, K. *J. Colloid Interface Sci.* **1994**, *165*, 532.
(20) Kevan, L. *Acc. Chem. Res.* **1987**, *20*, 1.
(21) Kevan, L. In *Time Domain Electron Spin Resonance*; Kevan, L., Schwartz, R. N., Eds.; Wiley: New York, 1979; p 279.
(22) Luan, Z.; He, H.; Zhou, W.; Cheng, C. F.; Klinowski, J. *J. Chem. Soc., Faraday Trans.* **1995**, *91*, 2955.
(23) Schmidt, R.; Junggreen, H.; Stöcker, M. *Chem. Commun.* **1996**, 875.
(24) Brunauer, S.; Deming, L. S.; Deming, W. S.; Teller, E. *J. Am. Chem. Soc.* **1940**, *62*, 1723.
(25) Ovchinnikov, I. V.; Konstantinov, V. N. *J. Magn. Reson.* **1978**, *32*, 179.
(26) Tominage, H.; Ono, Y.; Keii, T. *J. Catal.* **1975**, *40*, 1075.
(27) Hathaway, B. J.; Billing, D. E. *Coord. Chem. Rev.* **1970**, *5*, 143.
(28) Yu, J. S.; Comets, J. M.; Kevan, L. *J. Phys. Chem.* **1993**, *97*, 11047.
(29) Ucun, F.; Koksal, F.; Tapramaz, R. *Zeolites* **1992**, *12*, 420.
(30) Sass, C. E.; Kevan, L. *J. Phys. Chem.* **1988**, *92*, 5192.
(31) Lee, C. W.; Chen, X.; Kevan, L. *J. Phys. Chem.* **1991**, *95*, 8682.
(32) Vansant, E. F.; Lunsford, J. H. *J. Phys. Chem.* **1972**, *76*, 2860.
(33) Anderson, M. M.; Kevan, L. *J. Phys. Chem.* **1987**, *91*, 2926.
(34) Haynes, H. W. *Catal. Rev. Sci. Eng.* **1978**, *17*, 273.
(35) Jacobs, P. A.; Mortier, W. J. *Zeolites* **1982**, *2*, 226.
(36) Dwyer, J. In *Innovation in Zeolite Materials Science*; Grobet, P. J., Mortier, W. J., Vansant, E. F., Schulz-Ekloff, G., Eds.; Elsevier: Amsterdam, 1988; p 333 [*Stud. Surf. Sci. Catal.* **1988**, *37*, 333].
(37) Knözinger, H.; Ratnasamy, P. *Catal. Rev. Sci. Eng.* **1978**, *17*, 31.
(38) Freude, D.; Hunger, M.; Pfeifer, H. *Chem. Phys. Lett.* **1986**, *128*, 62.
(39) Sauer, J.; Schirmer, W. In *Innovation in Zeolite Materials Science*; Grobet, P. J., Mortier, W. J., Vansant, E. F., Schulz-Ekloff, G., Eds.; Elsevier: Amsterdam, 1988; p 323 [*Stud. Surf. Sci. Catal.* **1988**, *37*, 323].
(40) Kawakami, H.; Yoshida, S.; Yonezawa, T. *J. Chem. Soc., Faraday Trans. 2* **1984**, *80*, 205.